Molecular Therapy
Original Article

miR-25 Tough Decoy Enhances Cardiac Function in Heart Failure

Dongtak Jeong,[1] Jimeen Yoo,[1] Philyoung Lee,[1] Sacha V. Kepreotis,[1] Ahyoung Lee,[1] Christine Wahlquist,[2] Brian D. Brown,[3] Changwon Kho,[1] Mark Mercola,[2] and Roger J. Hajjar[1]

[1]Cardiovascular Research Center, Icahn School of Medicine at Mount Sinai, New York, NY 10029, USA; [2]Department of Medicine and Cardiovascular Institute, Stanford University School of Medicine, Palo Alto, CA 94304, USA; [3]Genetics and Genomic Sciences, Icahn School of Medicine at Mount Sinai, New York, NY 10029, USA

MicroRNAs are promising therapeutic targets, because their inhibition has the potential to normalize gene expression in diseased states. Recently, our group found that miR-25 is a key SERCA2a regulating microRNA, and we showed that multiple injections of antagomirs against miR-25 enhance cardiac contractility and function through SERCA2a restoration in a murine heart failure model. However, for clinical application, a more stable suppressor of miR-25 would be desirable. Tough Decoy (TuD) inhibitors are emerging as a highly effective method for microRNA inhibition due to their resistance to endonucleolytic degradation, high miRNA binding affinity, and efficient delivery. We generated a miR-25 TuD inhibitor and subcloned it into a cardiotropic AAV9 vector to evaluate its efficacy. The AAV9 TuD showed selective inhibition of miR-25 *in vitro* cardiomyoblast culture. *In vivo*, AAV9-miR-25 TuD delivered to the murine pressure-overload heart failure model selectively decreased expression of miR-25, increased levels of SERCA2a protein, and ameliorated cardiac dysfunction and fibrosis. Our data indicate that miR-25 TuD is an effective long-term suppressor of miR-25 and a promising therapeutic candidate to treat heart failure.

INTRODUCTION

Heart failure is the culmination of diverse cardiovascular diseases, including hypertension, ischemic disease, atherosclerosis, valvular insufficiency, myocarditis, and contractile protein mutations.[1] Despite varying etiologies and manifestations, heart failure is uniformly characterized by a progressive loss of contractile function and reserve. The prevailing therapeutic strategy is to block the deleterious effects of the renin-angiotensin and sympathetic systems, but existing drugs target few mechanisms within the failing cardiomyocyte and there is a critical need for novel drugs, especially in patients with advanced heart failure.[2,3] A complex intracellular network balances contractility and intracellular Ca^{2+} handling in relationship to workload and has been extensively modeled and reviewed.[4] However, the role of microRNAs (miRNAs) in these models remains largely unexplored. miRNAs are a family of small, non-coding RNAs that silence mRNA and regulate gene expression at the post-transcriptional level.[5,6] miRNAs evolved to fine-tune nearly all normal and pathological processes examined by downregulating proteins that occupy key nodal points.[7,8] We reasoned that miRNAs that repress contractility might be upregulated during human heart failure and might therefore constitute novel targets for therapeutic intervention.

The calcium-transporting ATPase SERCA2a, also known as ATP2A2, is the primary mechanism for Ca^{2+} uptake during excitation-contraction coupling in cardiomyocytes. Impaired Ca^{2+} uptake, resulting from decreased expression and reduced activity of SERCA2a, is a hallmark of heart failure.[9] Accordingly, restoration of SERCA2a by gene transfer has proved effective in improving key parameters of heart failure in animal models.[10] Although gene therapy clinical trials of AAV1.SERCA2a did not show beneficial effects in patients with heart failure (due to very low transduction efficiency), SERCA2a remains an important target.[11] Our group identified miR-25 as a significant suppressor of SERCA2a with pathological upregulation of endogenous miR-25 detected in human myocardial samples obtained from patients with severe heart failure.[12] In the same study, miR-25 inhibition via an antisense oligonucleotide (AO) antagomir proved to halt the progression of cardiac failure in mice that had undergone transverse aortic constriction (TAC) surgery. This antagomir was delivered systemically using nanoparticle technology, the major limitations of which include poor tissue specificity, with a limited duration of effect in the target organ. Therefore, the strong and stable suppression of specific miRNA activity would be essential to evaluate the therapeutic potential of such an approach. Numerous forms of antagomirs have been trialed in the past with various chemical modifications to confer increased nuclease resistance, higher binding affinity, improved delivery efficiency, and modulation of renal clearance.[13] Even with improvements in these parameters, however, Haraguchi et al.[14] proved that a more potent miRNA inhibition method exists. In their 2009 study, they tested various RNA decoy designs delivered via lentiviral vectors and established a precise configuration that achieved the most efficient and specific miRNA suppression. They coined this configuration Tough Decoy (TuD), which proved to possess the optimal arrangement of stem length and miRNA binding sites

Received 26 April 2017; accepted 22 November 2017;
https://doi.org/10.1016/j.ymthe.2017.11.014.

Correspondence: Roger J. Hajjar, MD, Cardiovascular Research Center, Icahn School of Medicine at Mount Sinai, One Gustave Levy Place, New York, NY 10029, USA.
E-mail: roger.hajjar@mssm.edu

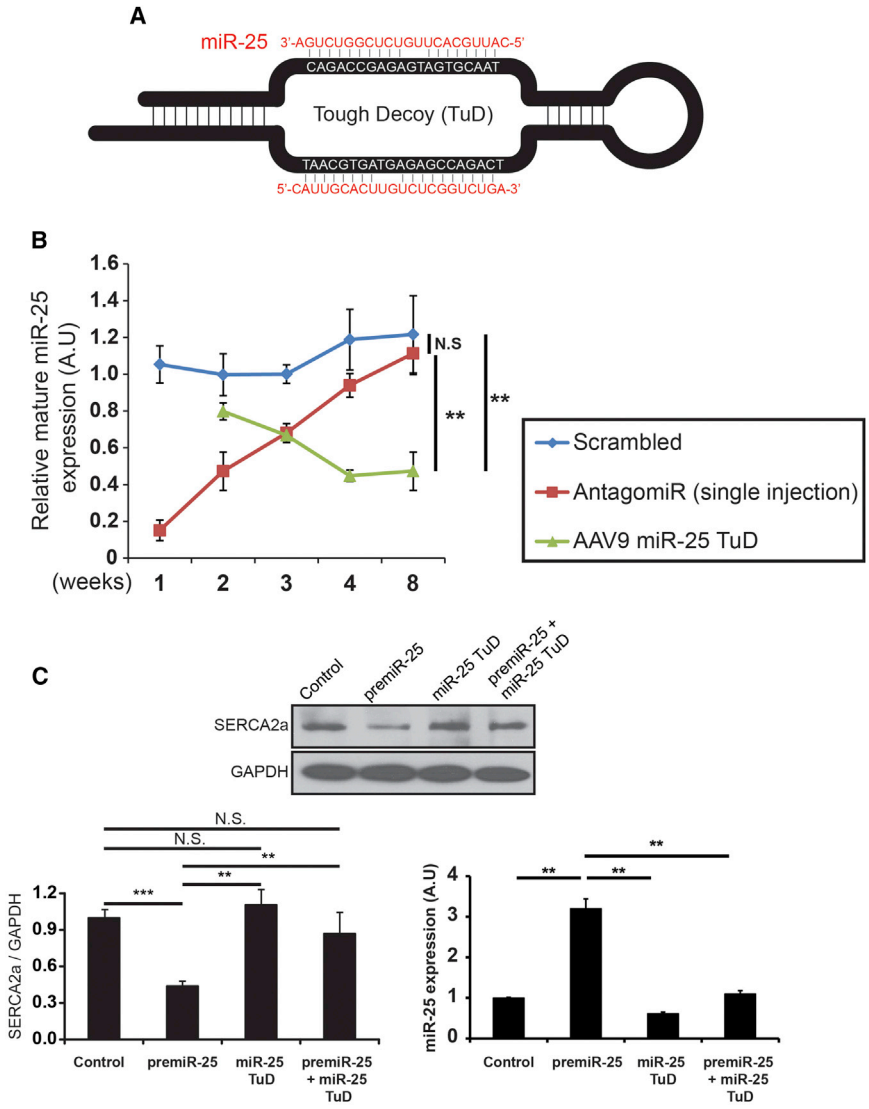

Figure 1. miR-25 Tough Decoy Generation and Evaluation

(A) miR-25 TuD was generated. (B) Single injection of miR-25 antagomir over 8 weeks showed significantly reduced relative mature miR-25 expression compared to AAV9 miR-25 TuD. (C) Co-transfection of miR-25 TuD with pre-miR-25 significantly abolished the restoration of SERCA2a, and transfection of miR-25 TuD in H9c2 showed significantly attenuated miR-25 expression. All data are represented as means ± SD (**p < 0.01, ***p < 0.005).

with the linker sequence between.[14] Proved to be superior to chemically modified oligonucleotides and Sponge Decoys, the TuD is the most effective method of miRNA inhibition.[15] When delivered through a viral vector, TuD confers the longest duration of miRNA suppression.[16] Using this method, we have successfully generated miR-25 TuD and combined it with the adeno-associated virus (AAV) serotype 9 (AAV9) system to achieve long-term activity. We hypothesize that stable inhibition of miR-25 will result in improved cardiac function in the setting of heart failure (HF) through improvements in cardiomyocyte Ca^{2+} handling.

RESULTS

Generation of miR-25 TuD

TuD libraries and the miR-25 TuD sequence (Figure 1A) were generated as previously described.[17] miR-25 TuD was inserted into a self-complementary AAV plasmid under the U6 promoter to generate a cardiotropic AAV9 virus. The duration of transgene expression and inhibitory effect of miR-25 TuD expression in the heart was followed for eight weeks post-intravenous injection. Compared to antagomir, AAV9 miR-25 TuD showed superior inhibitory activity (**p < 0.01) (Figure 1B). To establish the effect of miR-25 TuD against its target, functionality was confirmed via transfection experiments using H9c2 cells and qRT-PCR was conducted to measure miR-25 expression. The level of mature miR-25 expression was dramatically attenuated by miR-25 TuD transfection (**p < 0.01) (Figure 1C). Western blot analysis confirmed that miR-25 TuD nearly restored SERCA2a levels, which were blocked by transfection of pre-miR-25 (**p < 0.01) (Figure 1C).

Effect of miR-25 TuD *In Vitro*

To evaluate the effect of miR-25 TuD, we first validated miR-25 TuD specificity and binding efficiency against SERCA2a 3′ UTR using a luciferase assay system (Figure 2A). Luciferase activity was significantly reduced by miR-25 TuD transfer in a dose-dependent manner (***p < 0.005) (Figure 2B) in both HEK293 and H9c2 cells. Luciferase activity in miR-25 TuD-treated H9c2 cells was higher than that transfected with control plasmid. SERCA2a expression also dramatically increased in miR-25 TuD-transferred H9c2 cells (Figure 2C).

In addition, we observed angiotensin II regulation of pre- and mature miR-25 expression. Calcium dysregulation was recapitulated *in vitro* using angiotensin II in H9c2 cells. Angiotensin II induced SERCA2a downregulation and a NCX upregulation trend (SERCA2a, p < 0.005; NCX, p = 0.072) (Figure S1), which mirrored heart failure molecular signaling (Figure S2). A representative *in vitro* figure is shown in Figure 2D, and original blots for Figure 2D and Figure S1 are shown in Figure S3. We observed that angiotensin II upregulates both pre- and mature miR-25 expression, which is normalized by miR-25 TuD transfer in H9c2 cells (***p < 0.001, **p < 0.005) (Figures 2E and 2F).

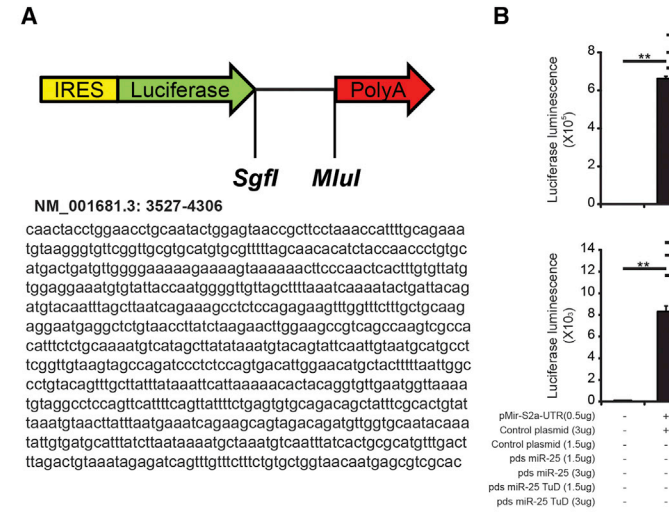

Figure 2. Effect of miR-25 TuD *In Vitro*

(A) miR-25 TuD specificity and binding efficiency against SERCA2a 3′ UTR was assessed using a luciferase assay system. (B) Luciferase assay shows significant reduced activity by miR-25 in a dose-dependent manner in both HEK293 and H9c2. (C) miR-25 TuD transfection shows restoration of SERCA2a in H9c2 cells. (D) Recapitulation of calcium dysregulation *in vitro* using angiotensin II in H9c2 cells shows SERCA2a downregulation and NCX upregulation. (E) Angiotensin II upregulates pre-miR-25 and is normalized by miR-25 TuD transfer in H9c2. (F) Angiotensin II upregulates mature-miR-25 and is normalized by miR-25 TuD transfer in H9c2. All data are represented as means ± SD (**p < 0.01, ***p < 0.005).

Cardiac Function Is Enhanced by miR-25 TuD Transfer

Next, we evaluated the effect of miR-25 TuD in a pressure-overload murine HF model using the AAV9 miR-25 TuD construct shown in Figure 3A. HF was initiated by TAC and monitored by serial echocardiography (see Materials and Methods). We have used extreme HF models for this study with TAC surgery, which showed significant reduction in both SERCA2a and NCX expression (Figure S2). After confirming cardiac dysfunction, AAV9 was injected intravenously with a concentration of 5×10^{11} vg per mouse. Genomic incorporation showed significant AAV9 control and miR-25 TuD within the mice genomes ($p < 0.005$, n = 5 each) (Figure S4).

Echocardiogram Results

Representative echocardiographic figures are shown in Figure 3B. Eight weeks after TAC surgery, fractional shortening significantly decreased, reflecting heart failure (**p < 0.005) (Figure 3C). These mice were randomly treated with either AAV9 control or AAV9 miR-25 TuD, and their cardiac function was observed 16 weeks after TAC surgery. AAV9 control-treated HF mice initially had an average fractional shortening of 38.21% ± 3.73% (n = 8), which deteriorated to 16.19% ± 0.86% (n = 5) eight weeks post-injection. In contrast, the AAV9 miR-25 TuD-treated HF group began with an average fractional shortening of 34.43% ± 6.08% (n = 5), which was maintained up to eight weeks after gene transfer. When both treatments were compared, AAV9 miR-25 TuD transfer resulted in statistically significant improvement in cardiac fractional shortening (*p < 0.05) (Figure 3C).

Invasive Hemodynamics Results

Pressure-volume loop multi-beat analysis after inferior vena cava occlusion in HF mice that had previously received either AAV9 control or AAV9 miR-25 TuD transfer showed an average end-systolic pressure-volume relationship (ESPVR) value of 2.17 ± 0.45 (n = 8) or 5.62 ± 0.73 (n = 8), respectively (**p < 0.005, *p < 0.05) (Figure 3D). Furthermore, dP/dt_{Max} significantly increased from 3,251 ± 841 (n = 8) in AAV9 control mice to 7,324 ± 1,048 (n = 5) in AAV9 miR-25 TuD-transferred mice (*p < 0.05) (Figure 3D). Average end-diastolic pressure-volume relationship (EDPVR) values of HF mice showed decreased values from 0.34 ± 0.06 (n = 5) in AAV9 control mice to 0.12 ± 0.04 (n = 5) in AAV9 miR-25 TuD-transferred mice (***p < 0.001, **p < 0.005) (Figure 3E). Diastolic value Tau showed significantly decreased values from 10.34 ± 2.12 (n = 5) in AAV9 control mice to 8.31 ± 1.77 (n = 5) in AAV9 miR-25 TuD-transferred mice (*p < 0.05) (Figure 3E).

Moreover, western blot analysis data support that SERCA2a expression was restored by miR-25 TuD transfer (***p < 0.001,

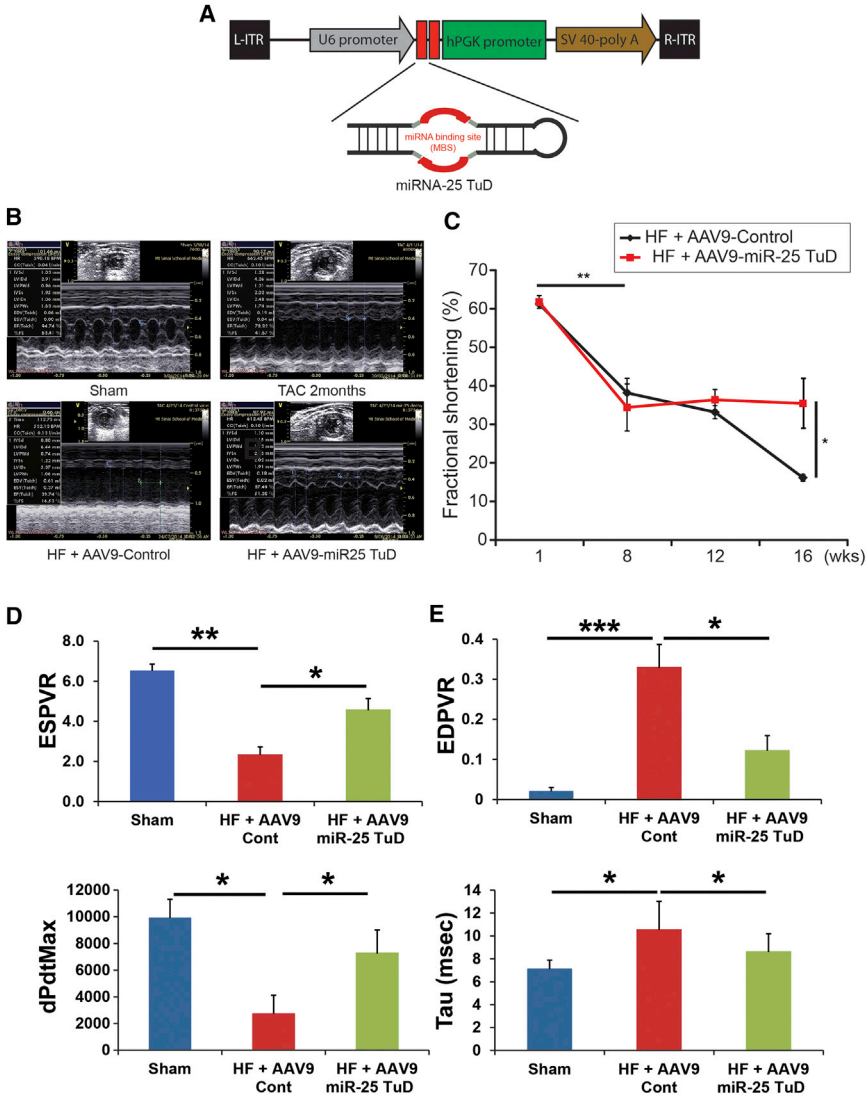

Figure 3. Cardiac Function Is Enhanced by miR-25 TuD Transfer

(A) miR-25 TuD construct subcloned into self-complementary AAV plasmid under U6 promoter. (B) Representative echocardiograms of sham, two months post-TAC, HF mouse with AAV9 control transfer, and HF mouse with AAV9 miR-25 TuD transfer. (C) AAV9 miR-25 TuD transfer significantly improves cardiac fractional shortening. (D) Hemodynamic data show systolic values ESPVR and dP/dt_{Max} significantly improved end-systolic elastance and myocardial contractility and global contractility. (E) Hemodynamic data show diastolic function EDPVR and Tau significantly decreased, indicating improved compliance and diastolic relaxation. All data are represented as means ± SD (*p < 0.05, **p < 0.01, ***p < 0.005).

p < 0.005, *p < 0.05) (Figure 4A), and northern blot and qRT-PCR data show that mature miR-25 expression was significantly induced in the HF group, which was substantially reduced by miR-25 TuD transfer (*p < 0.001, **p < 0.005) (Figures 4B and 4C). The original northern blot is shown in Figure S3.

miR-25 Is SERCA2a Specific, with No Cross Reactivity with Other Calcium Signaling Proteins

Western blot analysis was performed to evaluate calcium regulatory proteins such as SERCA2a, phospholamban (PLN), NCX, RyR, and IP3R2 (Figure 5; Figure S5). SERCA2a expression and PLN phosphorylation were significantly enhanced in miR-25 TuD-transferred mice (**p < 0.005 and *p < 0.05, respectively) (Figure 5). NCX, RyR, and IP3R2 expression remained unchanged among groups (Figure 5; Figure S5). These results align with our previous findings, which show a correlation between cardiac function and SERCA2a expression.[12] In addition, SUMO1 expression level was evaluated, because SUMO1 was reported as a critical modulator of SERCA2a in the post-translational process.[18] SUMO1 was significantly elevated by miR-25 TuD delivery (Figure S6). We assume that this could be an indirect effect, because miR-25 does not target SUMO1. Rather, this result is due to the restoration of SERCA2a. Moreover, miR-92a, a miR-17-92 member that has the same seeding sequence as miR-25, was measured to verify the target specificity of miR-25 TuD. miR-92a expression was altered by miR-25 TuD (Figure S7).

Cardiac Fibrosis Substantially Reduced by miR-25 TuD Transfer

Western blot analysis was performed to evaluate fibrosis markers Vimentin and α-SMA, in addition to endogenous antifibrotic molecule SMAD7 (Figure 6A). When compared to control, miR-25 TuD-treated mice showed decreasing trends in Vimentin expressions and significant decrease in α-SMA expression (**p < 0.005, *p < 0.05) (Figure 6A). Fibrosis inhibition molecule SMAD7 showed significant restoration from control to miR-25 TuD-treated mice (**p < 0.005, *p < 0.05) (Figure 6A). Masson trichrome staining of HF mice, which received AAV9 control compared to AAV9 miR-25 TuD transfer, showed significant decrease of fibrosis, aligning with western blot analysis (**p < 0.005, *p < 0.05) (Figure 6B). Furthermore, examination of apoptosis-related signaling molecules Bcl-2, BAX, and caspase-3 showed these to be significantly blunted by miR-25 TuD transfer (**p < 0.005, *p < 0.05) (Figure 6A). TUNEL staining of HF mice that which received AAV9 control compared to AAV9 miR-25 TuD transfer showed decrease in apoptosis signaling, aligning with western blot analysis (Figure 6C).

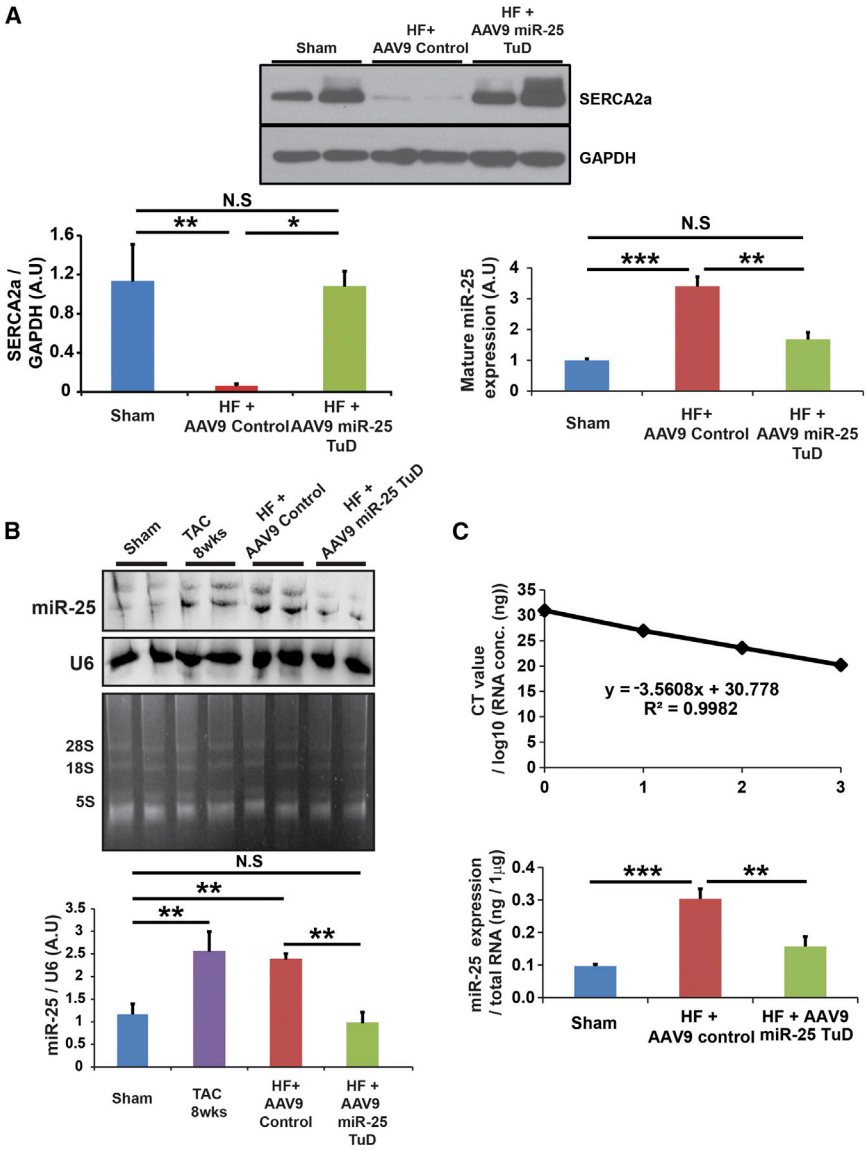

Figure 4. SERCA2a Expression Is Restored by miR-25 TuD

(A) miR-25 TuD transfer restored SERCA2a expression. Mature miR-25 expression is significantly induced in HF with AAV9 control-transferred mice and significantly reduced in HF with miR-25 TuD-transferred mice. (B) Northern blot of miR-25 was normalized by U6. Polyacrylamide gel before transfer shows 8S, 18S, and 28S bands clearly, showing limited degradation. Quantification shows that miR-25 increases as HF progresses. However, after AAV9 miR-25 TuD transfer, miR-25 levels significantly decrease. (C) qRT-PCR data show that miR-25 expression increases in HF mice with AAV9 control transfer and decreases in HF mice with AAV9 miR-25 TuD transfer. Threshold cycles are plotted against the number of RNA concentration as a standard curve. All data are represented as means ± SD (*$p < 0.05$, **$p < 0.01$, ***$p < 0.005$).

The Activity of miR-25 TuD Transfer Is Blunted in SERCA2a KO Mice

To confirm that the effect of the miR-25 TuD requires SERCA2a, we administered AAV9 miR-25 TuD or control (empty vector) intravenously to wild-type (WT) mice or Serca2a-cardiomyocyte null (S2a knockout [KO]) mice, as shown in the experimental protocol in Figure 7A. Echocardiogram showed that miR-25 TuD transfer had no effect on cardiac function in SERCA2a KO mice (Figure 7B). miR-25 TuD decreased endogenous miR-25 levels in WT and SERCA2a KO mice relative to control-treated animals (**$p < 0.005$, *$p < 0.05$) (Figure 7C). Nevertheless, because SERCA2a is absent in SERCA2a KO hearts (Figure 7D), SERCA2a protein levels were unaltered by miR-25 TuD treatment on both groups, although miR-25 expression level is substantially increased in SERCA2a KO mice, as shown in previous literature.[12]

miR-25 TuD Transfer Shows Anti-fibrotic Properties in SERCA2a KO Mice

To confirm that the effect of the miR-25 TuD may be due to additional binding partners, we observed miR-25 TuD on SERCA2a KO mice, as shown in the experimental protocol (Figure 8A). Western blot data showed significant increase in SMAD7 and decreasing trends of ColIA2 and α-SMA in AAV9 miR-25 TuD-transferred mice compared to control (***$p < 0.001$, *$p < 0.05$) (Figure 8D). Original blots for SERCA2a and SMAD7 are shown in Figure S3. Masson trichrome staining of SERCA2a KO HF mice, which received AAV9 control compared to AAV9 miR-25 TuD transfer, aligned with western blot data (Figure 8C). qRT-PCR data showed that mature miR-25 expression, as well as fibrosis markers transforming growth factor β1 (TGF-β1), Vimentin, and ColIA2, was significantly induced in the AAV9 control group (**$p < 0.005$, *$p < 0.05$) (Figure 8B), and all were significantly reduced by miR-25 TuD transfer except ColIA2 (*$p < 0.05$) (Figure 8B).

DISCUSSION

We previously reported that inhibition of endogenous miR-25 has a beneficial effect on cardiac function in the setting of heart failure.[12] Although the structure and chemistry of antagomirs have improved, they confer transient expression and need to be administered multiple times.[19,20] TuDs represent an improved anti-miRNA strategy, because the unique bulging structure of TuD protects it from endonucleolytic targeting.[21] Therefore, we generated a TuD inhibitor against miR-25 and delivered it with the AAV9 vector system to achieve cardiac specificity and long-term expression. We conducted this study to assess the potency of miR-25 inhibition using the AAV9 miR-25 TuD vector, specifically monitoring the effect of miR-25 inhibition on

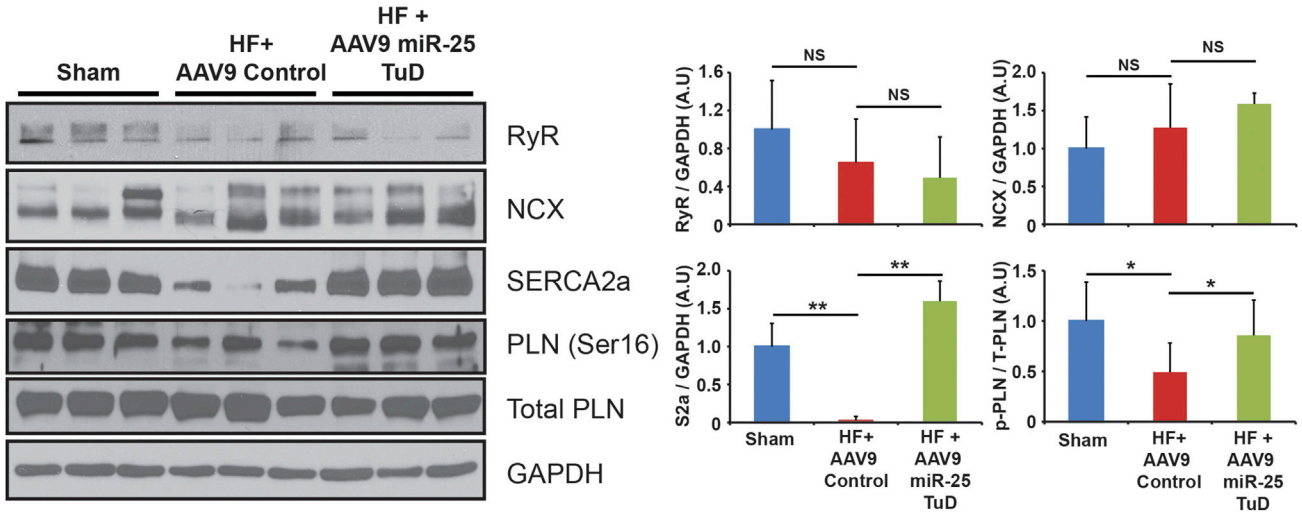

Figure 5. miR-25 Is SERCA2a Specific, with No Cross Reactivity with Other Calcium Signaling Proteins

SERCA2a and PLN phosphorylation were significantly enhanced in miR-25 TuD-transferred mice with NCX, and RyR expression remaining unchanged among groups. All data are represented as means ± SD (*$p < 0.05$, **$p < 0.01$).

SERCA2a levels and, in turn, cardiac function in the murine pressure-overload HF model. Because SERCA2a is a critical regulator of calcium homeostasis in HF and is negatively regulated by miR-25, we reasoned that the stable inhibition of miR-25 using TuD should have long-term beneficial effects on cardiac function.

We compared antagomir and TuD constructs in terms of transience of gene expression. Eight weeks after a single injection, miR-25 expression was significantly restored in the miR-25 antagomir-treated mice compared to those treated with miR-25 TuD (Figure 1B). For the inhibition of miR-25, miR-25 TuD had superior tissue specificity and longer transgene duration. The stability of TuD makes it a preferable method to antagomir in the case of miR-25. Our results show that the combination of AAV9-TuD against miR-25 is a potent suppressor of cardiac miR-25 levels, as determined by both qPCR and western blot (Figures 1C and 2B). This correlated with a subsequent increase in total SERCA2a levels (Figures 1C and 2C).

With respect to cardiac function, TAC-induced HF mice that received AAV9 miR-25 TuD showed an overall improvement in average fractional shortening from 34.43% ± 6.08% (n = 5) pretreatment to 35.46% ± 11.26% (n = 5) at the end of the experimental period, 8 weeks after gene transfer. HF mice that received AAV9 control started the experimental period with an average fractional shortening of 38.21% ± 3.73% (n = 8). This deteriorated to 16.19% ± 0.86% (n = 5) by the 8 week time point. Altogether, AAV9 miR-25 TuD transfer resulted in an improvement in fractional shortening compared to control ($p < 0.01$) (Figure 3C).

Our invasive hemodynamic data correlated with our echocardiographic findings, with multi-beat analyses of pressure-volume loops after inferior vena cava occlusion showing improved ESPVR in miR-25 TuD transfer, indicating overall improvement in end-systolic elastance and myocardial contractility ($p < 0.05$) (Figure 3D). In addition, improvement of dP/dt_{Max} showed improved global contractility ($p < 0.05$) (Figure 3D). Diastolic function was additionally analyzed, which showed a significant decrease in EDPVR, indicating an improvement in diastolic function through increased compliance ($p < 0.01$) (Figure 3E). Further analysis of our hemodynamic data showed a decrease in Tau, indicative of enhancement of diastolic relaxation ($p < 0.05$) (Figure 3E). miR-25 TuD treatment indicates overall improvement in both systolic and diastolic function through improved inotropic response and improvement in cardiac response under stress conditions.

To understand the molecular mechanisms of the functional improvement, we focused first on SERCA2a expression, which was restored by miR-25 TuD transfer ($p < 0.05$) (Figure 4A). Northern blot and qRT-PCR correlated with our western blot analysis, showing reduced miR-25 TuD transfer reduced the mRNA level of mature miR-25 ($p < 0.005$) (Figures 4B and 4C). We found no significant changes in NCX, RyR, and IP3R2 in response to miR-25 TuD transfer, indicating specificity for cardiac SERCA2a (Figure 5; Figure S5).

Phosphorylation of PLN, a negative regulator of SERCA2a function, was also substantially increased, suggesting improved calcium regulation ($p < 0.05$) (Figure 5).[22–24] This result aligns with our previous findings, which show a correlation between cardiac function and SERCA2a expression.[12] Altogether, these data indicate that AAV9 miR-25 TuD significantly enhances cardiac function through SERCA2a restoration. This conclusion is supported by the finding that AAV9 miR-25 TuD altered miR-25 expression levels but did not affect cardiac function in SERCA2a KO mice (Figures 7B–7D).

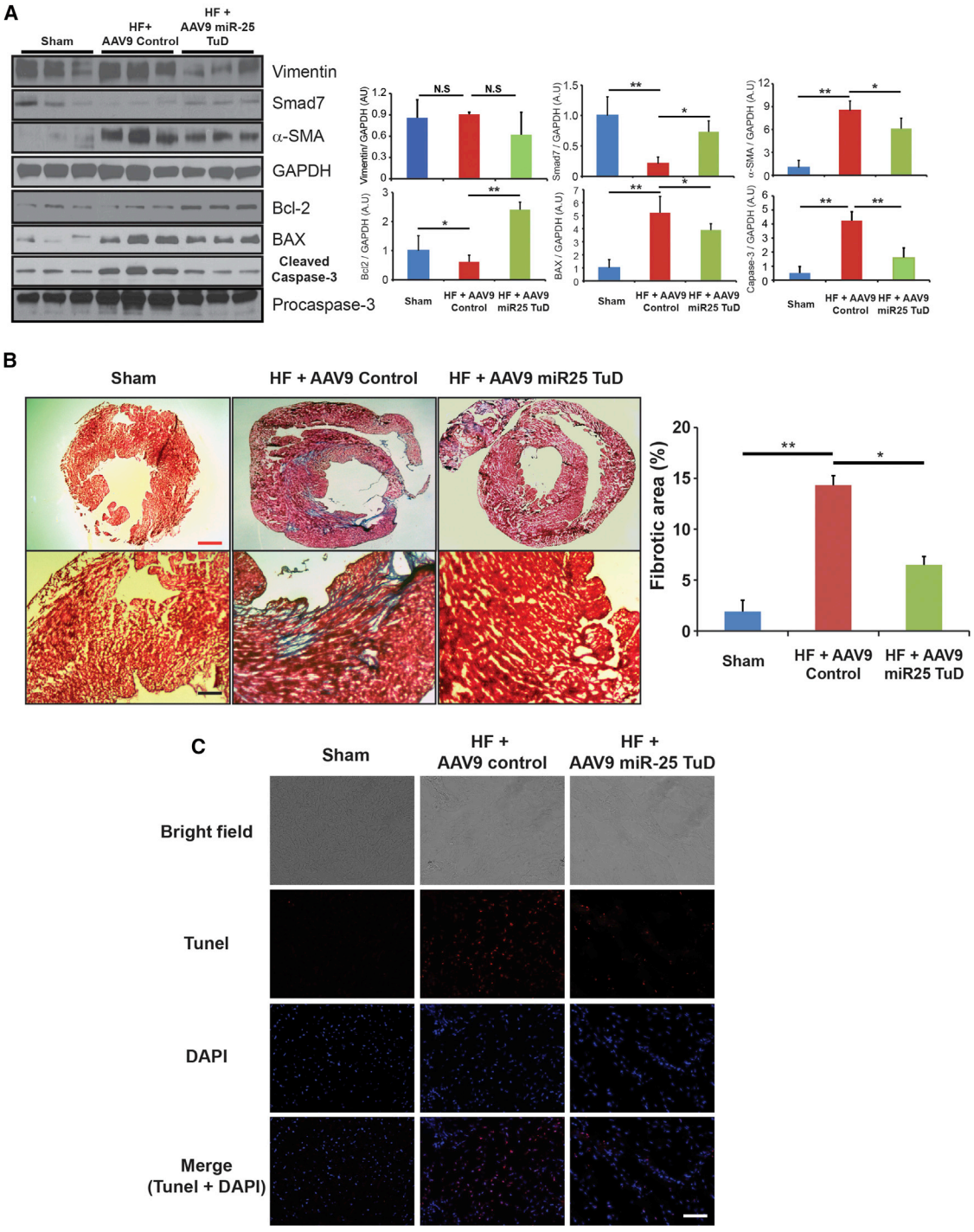

Figure 6. miR-25 TuD Transfer Substantially Reduces Cardiac Fibrosis and Apoptosis-Related Signaling Molecules

(A) Fibrosis markers, Vimentin, and α-SMA showed decreasing trends, but fibrosis inhibition marker SMAD7 showed significant restoration from control to miR-25 TuD-treated mice. In addition, apoptosis signaling molecules Bcl-2, BAX, and caspase-3 were significantly blunted by miR-25 TuD transfer. (B) Masson trichrome staining of HF mice showed significant decrease in fibrosis in miR-25 TuD-transferred mice compared to AAV9 control-transferred mice. (C) TUNEL staining was conducted to visualize apoptosis signaling in sham and HF mice treated with AAV9 control or AAV9 miR-25 TuD. All data are represented as means ± SD (*$p < 0.05$, **$p < 0.01$). Red scale bar, 1 mm; black scale bar, 50 μm; white scale bar, 25 μm.

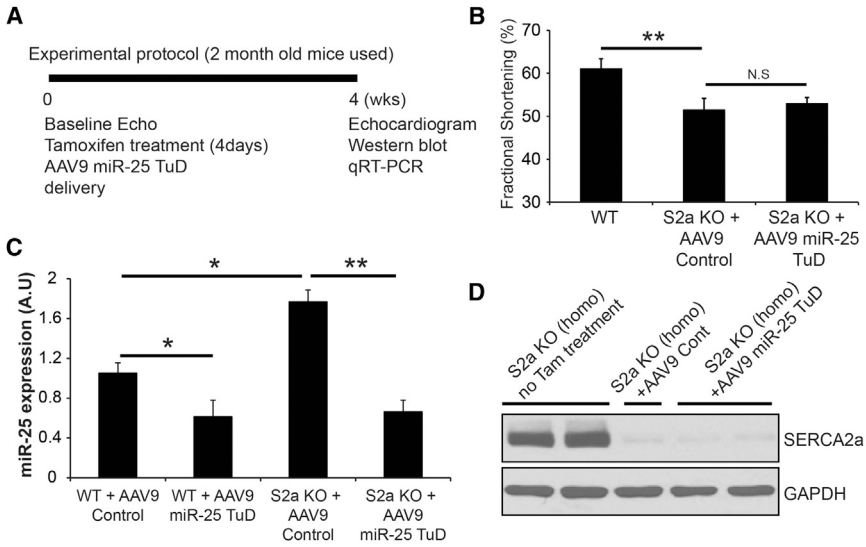

Figure 7. The Activity of miR-25 TuD Transfer Is Blunted in SERCA2a KO Mice

(A) Experimental protocol of miR-25 TuD transfer is shown. (B) Echocardiogram data showed that miR-25 TuD had no effect on cardiac function in SERCA2a KO mice. (C) miR-25 TuD decreased endogenous miR-25 levels in WT, and SERCA2 decreased endogenous miR-25 levels in WT and SERCA2a KO mice. (D) SERCA2a expression is unaltered by miR-25 TuD in both groups, although miR-25 expression level is substantially increased in SERCA2a KO mice. All data are represented as means ± SD (*$p < 0.05$, **$p < 0.01$).

In addition, degeneration of cardiomyocytes leads to significant fibrosis formation and thus a progressive decline in cardiac function.[25–27] Thus, fibrotic signaling markers were evident in the pressure-overload model. We observed a decreasing trend in fibrosis marker Vimentin and a significant decrease in fibrosis marker α-SMA following miR-25 delivery ($p < 0.05$) (Figure 6A).

Fibrosis inhibition marker SMAD7 significantly increased following miR-25 TuD delivery ($p < 0.05$) (Figure 6A). Masson trichrome staining showed significant decrease in fibrosis in miR-25 decoy-treated mice, in support of the western blot data ($p < 0.05$) (Figure 6B). We investigated miR-25 TuD delivery in SERCA2a KO mice to determine whether miR-25 TuD may have additional binding partners leading to decreased fibrosis. SMAD7 was significantly restored in miR-25 TuD-transferred mice ($p < 0.005$), and fibrosis markers ColIA2 and α-SMA were significantly reduced (Figure 8D). Masson trichrome staining aligned with this data (Figure 8C). Furthermore, qRT-PCR showed miR-25 decreased, in addition to fibrosis indicators TGF-β1, Vimentin, and ColIA2, which significantly decreased (Figure 8B). The significant change in fibrosis, more specifically, SMAD7, in both WT and SERCA2a KO mice raises the possibility that miR-25 may have other mRNA targets, in addition to SERCA2a, that are relevant to cardiac fibrosis.

This was validated with the finding that miR-25 TuD transfer resulted in reduction of pro-apoptotic marker expression. We saw significantly lower levels of Bcl-2 expression in HF mice when compared to WT ($p < 0.01$) (Figure 6A). This was shown to dramatically increase after receiving miR-25 TuD treatment ($p < 0.01$) (Figure 6A). Conversely, both BAX and cleaved caspase-3 were significantly elevated compared to WT ($p < 0.01$) (Figure 6A); however, both reduced significantly in response to miR-25 decoy transfer ($p < 0.05$ and $p < 0.01$, respectively) (Figure 6A). TUNEL staining also aligned with these results (Figure 6C). These molecular findings reflect a significant cardiomyocyte survival benefit and protection from pathological cardiac remodeling due to the inhibition of miR-25. The cumulative effects of these findings support the observation that AAV9 miR-25 TuD transfer results in the amelioration of cardiac dysfunction in TAC-induced HF mice.

In an era of rapidly expanding appreciation of epigenetics, miRNA inhibition is proving to be an increasingly influential method of gene modulation.[28] Thus far, improvement in cardiac function through the inhibition of miR-25 has only been tested using an antagomir in the surgical heart failure model, which reflects a pressure-overload cardiomyopathy.[12] Our study extends the current methodology through the refined union of a proficient miRNA inhibitor and the most cardiotropic viral vector available to maximize the efficiency and duration of transgene expression. We believe this demonstration has broader implications, because numerous cardiac miRNA targets have been identified and linked with pathological processes but to date have largely been studied through the use of chemically modified oligonucleotide inhibitors.[5,28–31] This study establishes a potent cardiotropic method of strong miRNA inhibition that has the potential to be applied to other miRNA therapeutic targets for cardiovascular disease.

MATERIALS AND METHODS

Generation of miR-25 TuD

TuD libraries and the miR-25 TuD sequence were as previously described.[17] Briefly, the entire TuD is made up of 112 base pairs. Stem I, the linker, the miRNA binding site, stem 2, and the loop are made up of 18, 3, 22, 8, and 4 base pairs, respectively. The two miRNA binding sites are the same 5′-CAGACCGAGAGTAGTGCAAT-3′, which binds to the complementary 5′-AUUGCACUUGUCUCGGUCUG-3′ miR-25 site (Figure 1A).

Anti-miRNA Administration

Anti-miR-25 (product code AM10584) and anti-miRNA negative control (product code AM17010) were purchased from Thermo Scientific (IL, USA). Separate solutions of anti-miR-25 and anti-miRNA

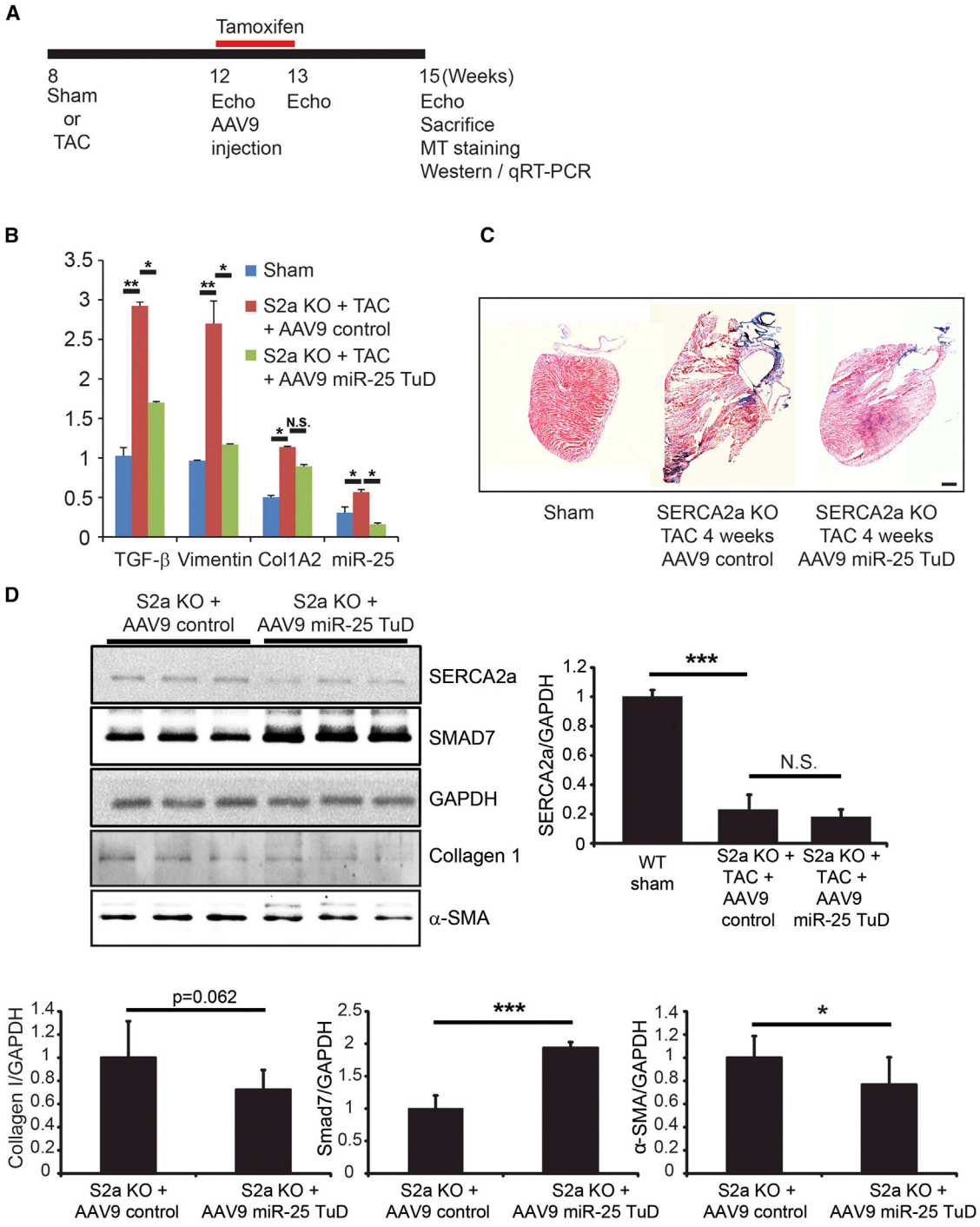

Figure 8. miR-25 Tough Decoy Transfer Shows Anti-fibrotic Properties in SERCA2a KO Mice

(A) Experimental protocol for SERCA2a KO HF mice treated with AAV9 control and miR-25 TuD is depicted. (B) qRT-PCR of miR-25 and fibrosis markers TGF-β, Vimentin, and ColIA2 are shown. In SERCA2a KO TAC mice treated with AAV9 control, both miR-25 and fibrosis markers significantly increase. miR-25 TuD treatment significantly decreases miR-25 and fibrosis markers. (C) Masson trichrome staining of SERCA2a KO TAC mice showed decrease in fibrosis in miR-25 TuD-transferred mice compared to AAV9 control-transferred mice. (D) Western blot shows a decreasing trend of collagen, a significant decrease of α-SMA, and a significant increase of SMAD7 between heart failure mice treated with AAV9 control and AAV9 miR-25 TuD. No significant changes were reported for SERCA2a. All data are represented as means ± SD (*$p < 0.05$, **$p < 0.01$, ***$p < 0.005$). Scale bar, 1 mm.

negative control were each diluted with *in vivo*-jetPEI solution (catalog no. 201-50, Polyplus-transfection, Illkirch, France) containing 10% (w/v) glucose at a ratio of *in vivo*-jetPEI nitrogen residues per oligonucleotide phosphate of 5, following the recommendations of the manufacturer. All solutions were mixed by vortexing for 10 s and incubated for at least 15 min at 37°C before injection. Each mouse received 400 mL of a saline and oligonucleotide mixture (100 mL of oligonucleotide solution plus 300 mL of saline, corresponding to 300 mg of oligonucleotide per dose) through tail vein injection. All injections were carried out using a 30-gauge needle syringe with a single mouse restrainer (Harvard Apparatus, MA, USA).

Cell Culture and Treatment

The H9c2 myoblast cell line, derived from embryonic rat heart, was obtained from ATCC (VA, USA). Cells were grown in DMEM (Thermo Scientific, IL, USA) with 10% heat-inactivated fetal bovine serum (FBS), penicillin (100 U/mL), and streptomycin (100 mg/mL), at 37°C in 5% CO_2 and 95% air, at a relative humidity of 95% and were split 1:4 at subconfluence (80%). Before each experiment, cells were seeded in six-well plates or chamber slides (NUNC 177437, Lab-Tek Chamber Slides, Thermo Scientific) at a density of 5×10^4 cells/cm^2 and starved for 18 hr in DMEM containing 0.1% FBS. H9c2 cells were treated with angiotensin II (10^{-7} M, Bachem, CA, USA) with or without miR-25 TuD plasmid transfection and pre-miR-25 for 4 days. They were used to verify the expression level of miR-25 and SERCA2a *in vitro*, followed by the same method we described earlier.

SERCA2a 3′ UTR Luciferase Assay

pMirtarget vector containing SERCA 3′ UTR was purchase from OriGene (MD, USA). SERCA2a 3′ UTR (NM_001681) was subcloned into pMirtarget vector using SgfI and MluI restriction enzymes as shown in Figure 2A. Both HEK293 cells and H9c2 rat cardiomyoblasts were used for luciferase assay. Cells were transfected using plasmids described in Figure 2B with polyethyleneimine (PEI) transfection reagent. After 24 hr, cells were harvested using lysis buffer from the Pierce Firefly Luciferase Glow Assay Kit (Thermo Scientific, IL, USA) and quantified by bovine serum albumin (BCA) assay reagents (Thermo Scientific, IL, USA). 10 μg of total lysate was used for each sample, and measurement was performed using a 1450 MicroBeta TriLux Microplate Scintillation and Luminescence Counter (PerkinElmer, CT, USA).

AAV Production

Self-complementary AAV (serotype 9) constructs were generated using the pds-AAV2-EGFP vector and the optimal TuD sequence against human miR-25. The EGFP sequence was removed from the AAV construct due to the side effect of GFP on cardiac function.[32,33] The recombinant AAV was produced by transfecting HEK293 T cells as described previously.[34] The AAV particles in the cell culture media were also collected by precipitation with ammonium sulfate and purified by ultracentrifugation on an iodixanol gradient. The particles were then concentrated by exchanging iodixanol for lactate Ringer's solution by multiple dilution and concentration steps using a centrifugal concentrator. The AAV titer was determined by real-time qPCR and SDS-PAGE.

Animal Care and Transverse Aortic Constriction

All procedures were approved by and performed in accordance with the Institutional Animal Care and Use Committee of the Icahn School of Medicine at Mount Sinai. The investigation conforms with the Guide for the Care and Use of Laboratory Animals published by the NIH (Publication No. 85-23, revised 1996). Studies were conducted in male B6C3F1 mice aged 8–10 weeks (weight, 25–30 g) obtained from Jackson Laboratory. Mice were anesthetized with a solution mixture of 95 mg/kg of ketamine and 5 mg/kg of xylazine administered via intraperitoneal injection. The mice were ventilated with a tidal volume of 0.2 mL and a respiratory rate of 110 breaths per minute (Harvard Apparatus). A longitudinal incision of 2–3 mm was made in the proximal sternum to allow visualization of the aortic arch.

The transverse aortic arch was ligated between the innominate and the left common carotid arteries with an overlaid 27-gauge needle. The needle was then immediately removed, leaving a discrete region of constriction.

Production of SERCA2a KO Mice

Conditional SERCA2 KO mice were donated by G. Christensen.[35] The mice were generated by standard gene-targeting strategies to introduce *loxP* sites into introns 1 and 3 of the Serca2. For our studies, 8- to 10-week-old mice were injected intraperitoneally with 4-hydroxy (4-OH) tamoxifen (1 mg/day) (Sigma-Aldrich, MO, USA) for 4 days to induce cardiomyocyte-specific excision of the Serca2 gene sequences, essentially as described.[35,36]

Echocardiography and *In Vivo* Hemodynamic Analysis

Mice were anesthetized by intraperitoneal injection of ketamine (100 μg/g). Two-dimensional images and M-mode tracings were recorded on the short axis at the level of the papillary muscle to determine the percentage of fractional shortening and ventricular dimensions (GE Vivid 7 Vision, IL, USA). One day after echocardiography, *in vivo* hemodynamic analysis was performed using a 1.2 Fr pressure-volume conductance catheter (Scisense, Ontario, Canada). Mice were anesthetized by intraperitoneal injection of a mixture of urethane (1 mg/g), etomidate (10 μg/g), and morphine (1 μg/g) and were then intubated via a tracheotomy and mechanically ventilated at a tidal volume of 7 μL/g and 125 respirations/min. The pressure-volume catheter was placed in the left ventricle via an apical stab approach as previously described.[37] Pressure-volume data were analyzed using IOX2 software (EMKA Technologies).

Histological Examination of Cardiac Tissues

Mouse heart tissues were cryopreserved with optimum cutting temperature (OCT) compound (Tissue-Tek, Sakura Finetek, USA) and sectioned into 6 μm thick slices. To measure the fibrotic areas, a Masson trichrome staining kit (ab150686; Abcam, MA, USA) was used for staining of the sectioned hearts. The fibrotic areas stained

blue, and the normal tissue stained red. The fibrotic area was calculated as the ratio of the total area of fibrosis to the total area of the section using ImageJ software (NIH, MD, USA). To detect apoptosis, TUNEL assay was conducted with the DeadEnd Fluorometric TUNEL kit (Promega, WI, USA) according to the manufacturer's instructions. Slides were sealed with glass slides using mounting medium with DAPI (Vectashield, CA, USA).

Western Blot Analysis

Membrane and tissue homogenates were prepared as previously described.[12] Proteins were resolved on 10% SDS-PAGE gels followed by transfer to polyvinylidene fluoride (PVDF) membranes (Millipore, MA, USA). Detection of the proteins bands was performed according to standard lab protocols.

Antibody raised against SERCA2a, RyR, NCX, CCN5, ColIA2, and GAPDH were purchased from Sigma-Aldrich (Seattle, USA), and antibodies raised against p-PLN(ser16), total PLN, p-caspase-3, caspase-3, Bcl-2, BAX, α-SMA, and Vimentin were purchased from Cell Signal (MA, USA). SMAD7 was purchased from Lifespan Biosciences (WA, USA).

Northern Blot Analysis of Small RNAs

Total RNA was isolated from cardiac tissues with the mirVana miRNA Isolation Kit, with phenol (Ambion, USA). Four microgram of total RNA were separated on 15% urea-polyacrylamide gel and transferred to BrightStar positively charged nylon membranes (Invitrogen, USA). Biotin conjugated-oligonucleotide probes complementary to miR-25-3p and U6, positive control, were purchased from Exiqon (product 611961-370, 5′-TCAGACCGAGACAAGTGC AAT-3′, and product 699002-370, 5′-CACGAATTTGCGTGTC ATCCTT-3′, respectively). In addition, all reagents for northern blot analysis were from the NorthernMax Kit (Thermo Fisher, USA), and the experimental protocol was modified according to various previous literature to enhance the detection capacity.[38,39]

Real-Time qPCR

RNA was isolated using the RNeasy Mini Kit (QIAGEN, Hilden, Germany), and cDNA was synthesized using the Verso cDNA Synthesis Kit (Thermo Scientific, IL, USA) according to the manufacturer's protocol. Real-time qPCR was done with PerfeCTa SYBR Green FastMix, Low ROX (Quanta BioSciences, MA, USA). For miRNAs, transcript levels were determined by real-time PCR using a QuantiTect SYBR Green real-time PCR kit (QIAGEN, Valencia, CA). Small RNAs were isolated from samples with the *mir*Vana miRNA Isolation Kit (Thermo Scientific, IL, USA) according to the manufacturer's instructions. Quantitative assay for miRNAs were performed using the miRNA expression assay kit (Exiqon, MA, USA) with LNA PCR primer set (Catalog no. 203351 for miR-25-3p) and the UniSp6 total nucleic acid (TNA) spike-in control primer set. Reverse transcription was performed at 42°C for 60 min and inactivated for 5 min at 95°C, and cDNA was amplified in 10 μL reaction volumes using 10 pmol of primers for 40 cycles: 95°C for 10 s, 60°C for 15 s, and 72°C for 5 s. A spike-in control primer set (UniSp6) and one candidate endogenous control primer set (miR-103a-3p) were used as internal controls to calculate the relative abundance of mRNAs. Primer information can be found in Table S1.

Statistical Analysis

Statistical analyses were performed using Student's t test or two-way ANOVA. Significant differences are demonstrated by a single asterisk, which indicates $p < 0.05$; a double asterisk, which indicates $p < 0.01$; or a triple asterisk, which indicates $p < 0.005$. Data in the figures represent the mean ± SD.

SUPPLEMENTAL INFORMATION

Supplemental Information includes seven figures and one table and can be found with this article online at https://doi.org/10.1016/j.ymthe.2017.11.014.

AUTHOR CONTRIBUTIONS

D.J. designed the research, performed the experiments, analyzed the data, and wrote the paper. J.Y., P.L., A.L., and S.V.K. contributed in performing experiments and review the manuscript. B.D.B. designed the TuD construct. C.W., C.K., and M.M. served as scientific advisers. R.J.H. revised the data and performed a final revision of data.

CONFLICTS OF INTEREST

The authors declare no competing financial interests.

ACKNOWLEDGMENTS

This work is supported by NIH grants R01 HL117505, HL119046, HL129814, HL128072, HL131404, HL135093, and P50 HL112324 and a Transatlantic Fondation Leducq grant. C.K. was funded by NIH grant R00 HL116645. We acknowledge the Gene Therapy Resource Program (GTRP) of the National Heart, Lung, and Blood Institute, NIH, for providing the gene vectors used in this study.

REFERENCES

1. Bonow, R.O., Mann, D.L., Zipes, D.P., and Libby, P. (2011). Braunwald's Heart Disease (Saunders).
2. Mudd, J.O., and Kass, D.A. (2008). Tackling heart failure in the twenty-first century. Nature *451*, 919–928.
3. Shah, A.M., and Mann, D.L. (2011). In search of new therapeutic targets and strategies for heart failure: recent advances in basic science. Lancet *378*, 704–712.
4. Greenstein, J.L., and Winslow, R.L. (2011). Integrative systems models of cardiac excitation-contraction coupling. Circ. Res. *108*, 70–84.
5. Dangwal, S., and Thum, T. (2014). MicroRNA therapeutics in cardiovascular disease models. Annu. Rev. Pharmacol. Toxicol. *54*, 185–203.
6. He, L., and Hannon, G.J. (2004). MicroRNAs: small RNAs with a big role in gene regulation. Nat. Rev. Genet. *5*, 522–531.
7. Bartel, D.P. (2009). MicroRNAs: target recognition and regulatory functions. Cell *136*, 215–233.
8. Filipowicz, W., Bhattacharyya, S.N., and Sonenberg, N. (2008). Mechanisms of post-transcriptional regulation by microRNAs: are the answers in sight? Nat. Rev. Genet. *9*, 102–114.
9. Meyer, M., Schillinger, W., Pieske, B., Holubarsch, C., Heilmann, C., Posival, H., Kuwajima, G., Mikoshiba, K., Just, H., Hasenfuss, G., et al. (1995). Alterations of sarcoplasmic reticulum proteins in failing human dilated cardiomyopathy. Circulation *92*, 778–784.

10. Kawase, Y., Ly, H.Q., Prunier, F., Lebeche, D., Shi, Y., Jin, H., Hadri, L., Yoneyama, R., Hoshino, K., Takewa, Y., et al. (2008). Reversal of cardiac dysfunction after long-term expression of SERCA2a by gene transfer in a pre-clinical model of heart failure. J. Am. Coll. Cardiol. *51*, 1112–1119.

11. Jessup, M., Greenberg, B., Mancini, D., Cappola, T., Pauly, D.F., Jaski, B., Yaroshinsky, A., Zsebo, K.M., Dittrich, H., Hajjar, R.J., et al.; Calcium Upregulation by Percutaneous Administration of Gene Therapy in Cardiac Disease (CUPID) Investigators (2011). Calcium upregulation by percutaneous administration of gene therapy in cardiac disease (CUPID): a phase 2 trial of intracoronary gene therapy of sarcoplasmic reticulum Ca2+-ATPase in patients with advanced heart failure. Circulation *124*, 304–313.

12. Wahlquist, C., Jeong, D., Rojas-Muñoz, A., Kho, C., Lee, A., Mitsuyama, S., van Mil, A., Park, W.J., Sluijter, J.P., Doevendans, P.A., et al. (2014). Inhibition of miR-25 improves cardiac contractility in the failing heart. Nature *508*, 531–535.

13. Stenvang, J., Petri, A., Lindow, M., Obad, S., and Kauppinen, S. (2012). Inhibition of microRNA function by antimiR oligonucleotides. Silence *3*, 1.

14. Haraguchi, T., Ozaki, Y., and Iba, H. (2009). Vectors expressing efficient RNA decoys achieve the long-term suppression of specific microRNA activity in mammalian cells. Nucleic Acids Res. *37*, e43.

15. Bak, R.O., Hollensen, A.K., Primo, M.N., Sørensen, C.D., and Mikkelsen, J.G. (2013). Potent microRNA suppression by RNA Pol II-transcribed 'Tough Decoy' inhibitors. RNA *19*, 280–293.

16. Xie, J., Ameres, S.L., Friedline, R., Hung, J.H., Zhang, Y., Xie, Q., Zhong, L., Su, Q., He, R., Li, M., et al. (2012). Long-term, efficient inhibition of microRNA function in mice using rAAV vectors. Nat. Methods *9*, 403–409.

17. Mullokandov, G., Baccarini, A., Ruzo, A., Jayaprakash, A.D., Tung, N., Israelow, B., Evans, M.J., Sachidanandam, R., and Brown, B.D. (2012). High-throughput assessment of microRNA activity and function using microRNA sensor and decoy libraries. Nat. Methods *9*, 840–846.

18. Kho, C., Lee, A., Jeong, D., Oh, J.G., Chaanine, A.H., Kizana, E., Park, W.J., and Hajjar, R.J. (2011). SUMO1-dependent modulation of SERCA2a in heart failure. Nature *477*, 601–605.

19. Boutla, A., Delidakis, C., and Tabler, M. (2003). Developmental defects by antisense-mediated inactivation of micro-RNAs 2 and 13 in Drosophila and the identification of putative target genes. Nucleic Acids Res. *31*, 4973–4980.

20. Krützfeldt, J., Rajewsky, N., Braich, R., Rajeev, K.G., Tuschl, T., Manoharan, M., and Stoffel, M. (2005). Silencing of microRNAs in vivo with 'antagomirs'. Nature *438*, 685–689.

21. ter Brake, O., 't Hooft, K., Liu, Y.P., Centlivre, M., von Eije, K.J., and Berkhout, B. (2008). Lentiviral vector design for multiple shRNA expression and durable HIV-1 inhibition. Mol. Ther. *16*, 557–564.

22. Haghighi, K., Bidwell, P., and Kranias, E.G. (2014). Phospholamban interactome in cardiac contractility and survival: a new vision of an old friend. J. Mol. Cell. Cardiol. *77*, 160–167.

23. Kranias, E.G., and Hajjar, R.J. (2012). Modulation of cardiac contractility by the phospholamban/SERCA2a regulatome. Circ. Res. *110*, 1646–1660.

24. Kranias, E.G., and Hajjar, R.J. (2017). The phospholamban journey 4 decades after setting out for Ithaka. Circ. Res. *120*, 781–783.

25. Allen, D.G., Gervasio, O.L., Yeung, E.W., and Whitehead, N.P. (2010). Calcium and the damage pathways in muscular dystrophy. Can. J. Physiol. Pharmacol. *88*, 83–91.

26. Holland, A., and Ohlendieck, K. (2014). Proteomic profiling of the dystrophin-deficient mdx phenocopy of dystrophinopathy-associated cardiomyopathy. BioMed Res. Int. *2014*, 246195.

27. Shirokova, N., and Niggli, E. (2013). Cardiac phenotype of Duchenne muscular dystrophy: insights from cellular studies. J. Mol. Cell. Cardiol. *58*, 217–224.

28. Harada, M., Luo, X., Murohara, T., Yang, B., Dobrev, D., and Nattel, S. (2014). MicroRNA regulation and cardiac calcium signaling: role in cardiac disease and therapeutic potential. Circ. Res. *114*, 689–705.

29. Maegdefessel, L. (2014). The emerging role of microRNAs in cardiovascular disease. J. Intern. Med. *276*, 633–644.

30. Olson, E.N. (2014). MicroRNAs as therapeutic targets and biomarkers of cardiovascular disease. Sci. Transl. Med. *6*, 239ps3.

31. Small, E.M., and Olson, E.N. (2011). Pervasive roles of microRNAs in cardiovascular biology. Nature *469*, 336–342.

32. Agbulut, O., Coirault, C., Niederländer, N., Huet, A., Vicart, P., Hagège, A., Puceat, M., and Menasché, P. (2006). GFP expression in muscle cells impairs actin-myosin interactions: implications for cell therapy. Nat. Methods *3*, 331.

33. Huang, W.Y., Aramburu, J., Douglas, P.S., and Izumo, S. (2000). Transgenic expression of green fluorescence protein can cause dilated cardiomyopathy. Nat. Med. *6*, 482–483.

34. Kohlbrenner, E., and Weber, T. (2017). Production and characterization of vectors based on the cardiotropic AAV serotype 9. Methods Mol. Biol. *1521*, 91–107.

35. Andersson, K.B., Birkeland, J.A., Finsen, A.V., Louch, W.E., Sjaastad, I., Wang, Y., Chen, J., Molkentin, J.D., Chien, K.R., Sejersted, O.M., and Christensen, G. (2009). Moderate heart dysfunction in mice with inducible cardiomyocyte-specific excision of the Serca2 gene. J. Mol. Cell. Cardiol. *47*, 180–187.

36. Swift, F., Franzini-Armstrong, C., Øyehaug, L., Enger, U.H., Andersson, K.B., Christensen, G., Sejersted, O.M., and Louch, W.E. (2012). Extreme sarcoplasmic reticulum volume loss and compensatory T-tubule remodeling after Serca2 knockout. Proc. Natl. Acad. Sci. USA *109*, 3997–4001.

37. Pacher, P., Nagayama, T., Mukhopadhyay, P., Bátkai, S., and Kass, D.A. (2008). Measurement of cardiac function using pressure-volume conductance catheter technique in mice and rats. Nat. Protoc. *3*, 1422–1434.

38. Kim, S.W., Li, Z., Moore, P.S., Monaghan, A.P., Chang, Y., Nichols, M., and John, B. (2010). A sensitive non-radioactive northern blot method to detect small RNAs. Nucleic Acids Res. *38*, e98.

39. Várallyay, E., Burgyán, J., and Havelda, Z. (2008). MicroRNA detection by northern blotting using locked nucleic acid probes. Nat. Protoc. *3*, 190–196.